Structural Traits of Cuitzeo Lake, Central Mexico, and Areas of Geothermal Potential

Elizabeth Rivera-Calderón[1] and Román Alvarez[2]

Abstract

Cuitzeo Lake, in the central part of the Trans Mexican Volcanic Belt, is in an extensional region associated with the Cuitzeo graben, where magmatic ascent appears to provide the heat sources for the surface, geothermal manifestations. A profuse distribution of andesitic rocks is observed throughout the study area of 50×50 km². Gravity and magnetic field 3D inversions are calculated to obtain density and magnetic susceptibility distributions to 7000 m depth, from which we analyze N-S and E-W cross-sections and obtain density and magnetic susceptibility geosurfaces that help characterize anomaly areas of interest. We use satellite-derived gravity and magnetic data in our evaluation, owing to their high-resolution characteristics and uniform coverage of the study area. Analysis initiates with the San Agustín del Maíz region (SAM), exhibiting surface geothermal manifestations, to characterize its density and susceptibility characteristics, then the analysis is extended to the whole study area. Several outcropping, low magnetic susceptibility regions, like the one associated with SAM, are suggested as potential geothermal targets. Density geosurfaces point to two volumes where magmatic material may intrude, coinciding with active geologic faults. The analysis presented here can be extended to neighboring regions in the Cuitzeo Lake area and may constitute a fast, unexpensive exploration methodology in similar geothermal districts.

Resumen

El Lago de Cuitzeo se encuentra en la parte central del Cinturón Volcánico Trans Mexicano, en una región de extensión asociada al graben de Cuitzeo, en donde el ascenso magmático parece proporcionar las fuentes de calor que alimentan a las manifestaciones geotérmicas superficiales. Se observa una distribución profusa de andesitas a través del área de estudio de 50 × 50 km². Se calculan inversiones 3D de los campos de gravedad y magnético para obtener distribuciones de densidad y susceptibilidad magnética hasta 7000 m de profundidad, de las cuales obtenemos y analizamos secciones N-S y E-W, obteniendo también geo-superficies que ayudan a caracterizar las áreas de anomalía de interés. Utilizamos datos derivados de observaciones satelitales de gravedad y magnetismo debido a sus características de alta resolución y cobertura uniforme del área de estudio. El análisis se inicia con la región de San Agustín del Maíz (SAM), que exhibe manifestaciones geotérmicas superficiales, para caracterizar sus propiedades de densidad y susceptibilidad, y después el análisis se extiende a toda el área de estudio. Varios sitios en donde afloran regiones de baja susceptibilidad magnética, como en 46 el caso de SAM, se sugieren como blancos potenciales de exploración geotérmica. Dos geo-superficies de densidad apuntan a dos volúmenes en donde material magmático puede estar emplazado, coincidiendo con la presencia de fallas geológicas activas. El análisis presentado aquí puede extenderse a regiones vecinas al Lago de Cuitzeo, y pueden constituir una metodología de exploración rápida y económica en distritos geotérmicos similares.

Editorial responsibility: Dr. Marco Antonio Pérez-Flores

* Corresponding author: Román Alvarez, **roman.alvarez@iimas.unam.mx**

[1] Escuela Nacional de Estudios Superiores-Unidad Morelia, Universidad Nacional Autónoma de México, Antigua Carretera a Pátzcuaro 8701, C.P. 58190, Morelia, Michoacán, Mexico. **ecalderonzr@comunidad.unam.mx**

[2] Instituto de Investigaciones en Matemáticas Aplicadas y en Sistemas, Universidad Nacional Autónoma de México, Ciudad Universitaria, México DF, 04510, Mexico.

Elizabeth Rivera-Calderón, Román Álvarez-Bejar

Introduction

The geologic structure of Cuitzeo Lake is in the central part of Mexico (Figure 1), in the Trans Mexican Volcanic Belt (TMVB, Ferrari *et al.*, 2012) within the volcanic zone known as the Michoacán-Guanajuato Volcanic Field (Ferrari, 2000; Gómez-Vasconcelos *et al.*, 2015, 2020). Recent studies of the Cuitzeo Lake region have focused on the geothermal potential of this area (Gómez-Vasconcelos *et al.*, 2021a; Pola *et al.*, 2016; Trujillo-Hernández, 2017). Several geophysical studies reported anomalous behavior probably associated with magmatic ascent, related to the geothermal sources (Guevara-Alday, 2015). These sources are, in turn, related to the extensional phenomena associated with the Cuitzeo Lake graben (Israde-Alcantara & Garduño-Monroy, 1999; Garduño-Monroy *et al.*, 2009). Olvera-García *et al.*, (2020) established that this deep-seated geothermal system is buried under late Miocene-Holocene lacustrine sediments filling an extensional tectonic depression. Here, we focus on 2D and 3D, regional, gravity and magnetic field interpretations in this area, to highlight the main structural traits of the region to a depth of 7 km. Particular attention is given to areas with geothermal potential.

Regional geology

An extensional tectonic regime, with NNW orientation, originated the basin of Cuitzeo Lake in this volcanic region (Gómez-Vasconcelos *et al.*, 2021a; Gómez-Tuena *et al.*, 2007). Volcanic activity in the basin has been continuous since the Early Miocene to the Present; there are more than 50 volcanic chimneys, with associated structures such as scoria cones, lava domes, small shield volcanoes, and fissure lava flows (Israde-Alcantara & Garduño-Monroy, 1999; Garduño-Monroy *et al.*, 2009; Pola *et al.*, 2016; Trujillo-Hernández, 2017; Gómez-Vasconcelos *et al.*, 2020, 2021a;). The mountain landscape is conformed by ignimbrites, lava flows, pyroclastic and volcanoclastic deposits (Pola *et al.*, 2016), overlying a granitic basement (Trujillo-Hernández, 2017). Figure 2 shows the topography of the area, with Cuitzeo Lake exhibiting the lowest, regional elevations.

Tectonic activity in the central sector of the TMVB is indicated by widespread seismicity and earthquakes (M ≤ 5) with focal mechanisms ranging from transcurrent to normal (Quintanar *et al.*, 2004; Quintanar *et al.*, 2018; Suárez *et al.*, 2019).

The geologic map appears in Figure 3. This map represents the main regional geological units, the dominant geological faults are represented by the black lines. The main rock units are basalts, andesites, tuffs and ignimbrites that belong to the Sierra de Mil Cumbres and some from the Caldera de Atécuaro (Garduño-Monroy *et al.*, 2009). The topography of the area is conditioned by the structures of the Morelia-Acambay Fault System (Garduño-Monroy *et al.*, 2009; Gómez-Vasconcelos *et al.*, 2020; Israde-Alcantara & Garduño-Monroy, 1999) and the inferred Tzitzio-Valle de Santiago Fault. The semigraben and the graben of Cuitzeo can be observed in the central zone. The Morelia Acambay Fault System conditions the blocks of the
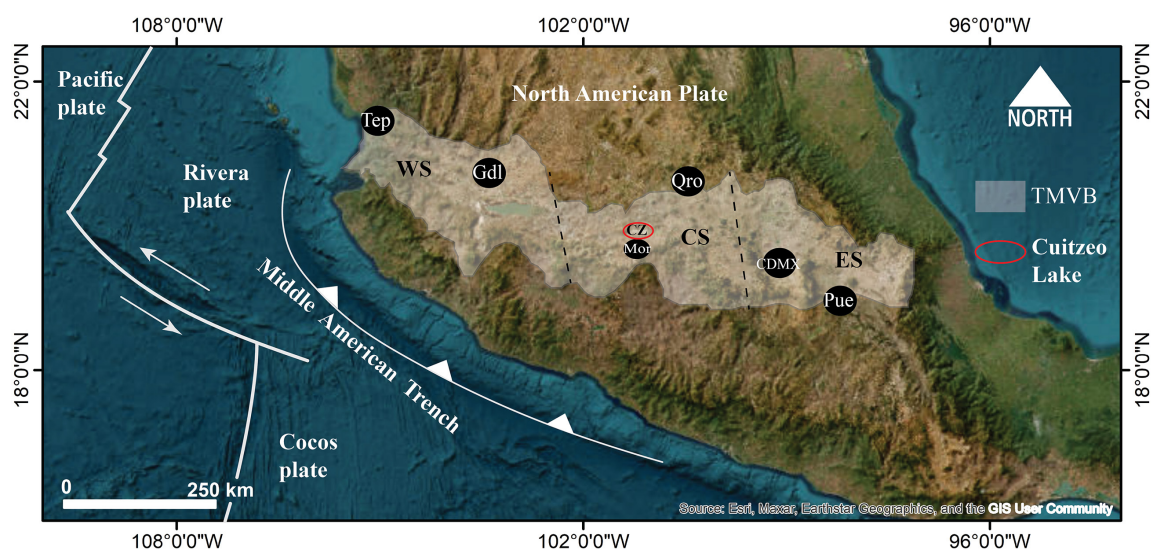

Figure 1. Location of Cuitzeo Lake (red ellipse) in the Central Sector (CS) of the Trans Mexican Volcanic Belt (TMVB, light brown). Parallel, dashed lines limit the sectors of the TMVB. CZ, Cuitzeo Lake. WS, Western Sector. ES, Eastern Sector (based on Correa-Gómez, 2019) . Tep, Tepic. Gdl, Guadalajara. Mor, Morelia. Qro, Querétaro. CDMX, Mexico City. Pue, Puebla.
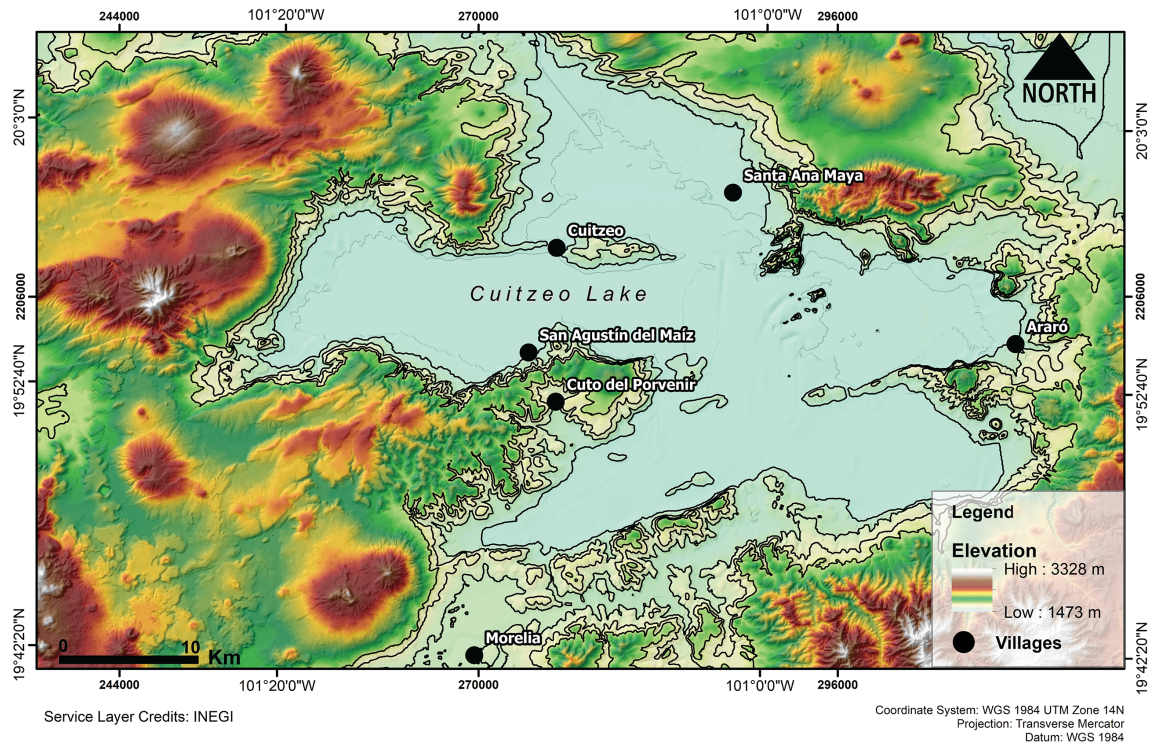
Figure 2. Topography around Cuitzeo Lake. Contours are at 50 m intervals between elevations of 1500 to 2000 m; these contours will be incorporated to the maps for reference. The highest elevation is at 2500 m. The lake is shallow, a few meters deep, and retreats considerably in some areas in the dry season. CU, Cuitzeo. AR, Araró, SAM, San Agustín del Maíz.
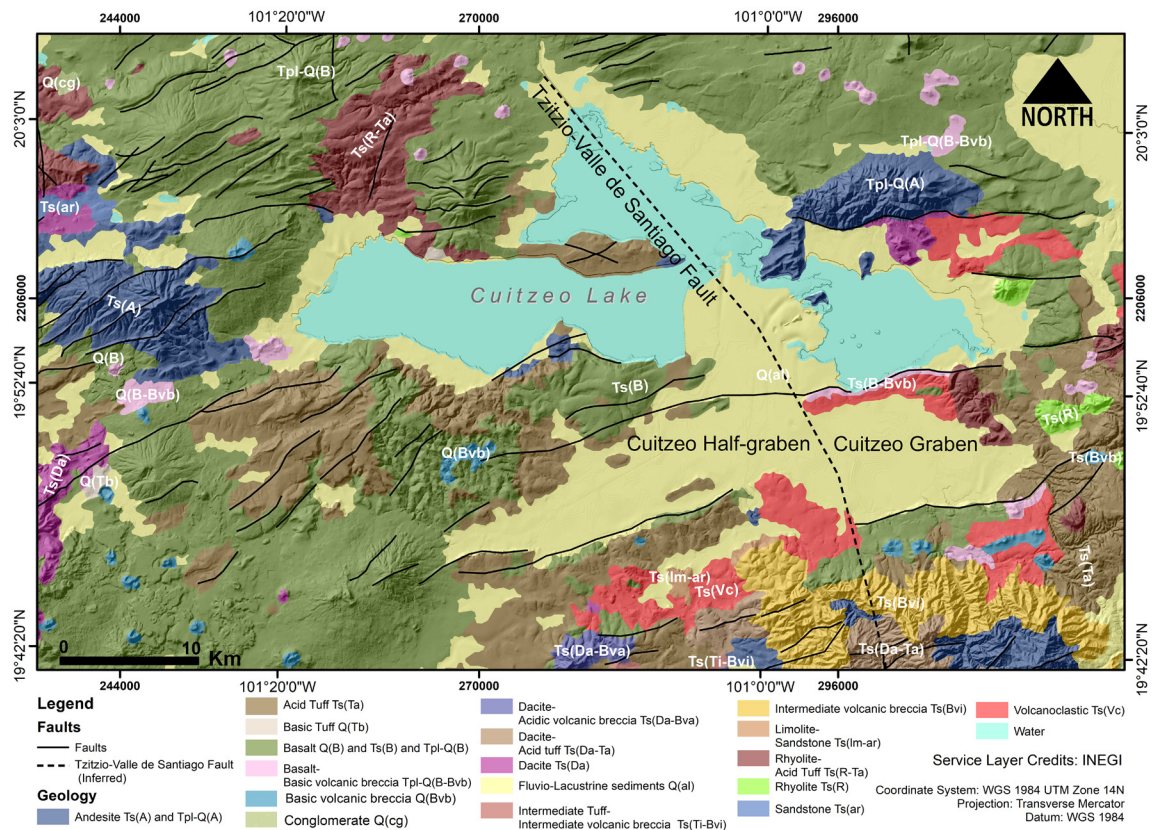

Figure 3. Regional, geologic map of the Morelia-Cuitzeo Lake region showing the Cuitzeo half-graben and graben, separated by the Titzio-Valle de Santiago Fault.

Cuitzeo graben, mainly conformed by normal and listric faults. In addition, they are the main zones of geothermal fluid ascent as in the case of SAM in the area of Cuitzeo Lake (Garduño-Monroy *et al.*, 2009; Israde-Alcantara & Garduño-Monroy, 1999; Olvera-García *et al.*, 2020).

Data acquisition

Gravity and magnetic data were obtained in the study area; magnetic data correspond to the North America Magnetic Field data set (NAMAG, 2002); they were reduced to the pole according to the standard procedure (Baranod & Naudy, 1964). The Bouguer gravity anomaly (simple) data were obtained from the EIGEN 6C4 satellite-derived data set of the International Centre for Global Earth Models (ICGEM, Barthelmes and Kohler, 2016), with a node separation of .01°. For the topography we used the Digital Elevation Model (DEM) of ASTER (**https://gdex.cr.usgs.gov/gdex/**) with a 30 m resolution. Bouguer anomaly (BA) was obtained by the classical gravity anomaly minus the attraction of the Bouguer plate, calculated by the spherical approximation of the classical gravity anomaly minus $2\pi G\rho H$, where the topographic heights $H(\lambda,\varphi)$ are calculated from the spherical harmonic model of topography (ETOPO1) used up to the same maximum degree as the gravity field model, with $\rho = 2670$ kg/m^3, and a resolution of 0.01°.

Figure 4 shows the magnetic map of the study area and Figure 5 shows the map corresponding to the gravity distribution. After the inversion process one obtains a distribution of magnetic susceptibilities in the case of the magnetic data, and a density distribution in the case of gravity data (Ellis *et al.*, 2012; MacLeod and Ellis, 2013). Various examples of 3D inversions are available (e.g., Alvarez & Yutsis, 2015; Alvarez & Yutsis, 2017; Guevara et al 2021; Camacho and Alvarez, 2021; Alvarez and Camacho, 2023).

The 3D inversion

We used the method described by Macleod and Ellis (2013) based on the theoretical considerations of Ellis *et al.* (2012) to perform the 3D inversions presented here. The code runs in the Oasis Montaj program of Geosoft, where a 3D mesh of parallelepipeds is established in the region to be inverted. The program uses a Cartesian Cut Cell algorithm (CCC) to represent geologic volumes whose values are modified to reach the observed gravity/magnetic response. An Iterative Reweighting Inversion algorithm (IRI, Ingram *et al.*, 2003) is used to match the observed results with the calculated ones within established

error limits; in the present cases is 5% of the standard deviation. It is expressed as the measure of errors between paired observations; in this case the gravity or magnetic field observed and the corresponding calculated field:

$$\sum_{i=1}^{n} |y_i - x_i| /n = \sum_{i=1}^{n} |e_i| /n$$

with

$$e_1 = |y_1 - x_i|$$

where y_i is the prediction and x_i is the true value.

The inversion results are provided as densities in g/cm^3 when making a gravity inversion, and magnetic susceptibility (SI units) when performing a magnetic inversion. The depth of the inverted volume is proportional to the size of the volume selected for the calculation. Typically, areas of 50×50 km^2 will attain depths of 5-6 km and greater depths can be obtained at the expense of the resolution. When referring to resolution we must bear in mind that there is the high-resolution of the data used to obtain the Bouguer anomaly in Figure 5a, in the gravity data case, and there is the resolution of the model proper. Models may have different dimensions and different resolutions; in this study we used models of dimensions in the X-Y plane of 1000 m, which we call the model resolution. To optimize computation, a subset of the high-resolution gravity data set is used, selected according to the model resolution, to perform the inversion. Figures 6a and 6b show the inverted volumes of the magnetic and the gravity inversions used in here; the latter shows the gravity station distribution used for that inversion.

Results

1) San Agustín del Maíz 1000m

We analyze first the region of San Agustín del Maíz (SAM), for its geothermal relevance. Olvera-García *et al.*, (2020) described its geothermal manifestations as distributed in an area characterized by fluvio-lacustrine sediments unconformably resting on volcanic rocks. They attribute the rising of geothermal fluids to permeable rock volumes located at the intersection of geologic fault systems where normal faults interact with transfer faults that together create rock zones of high permeability. High permeability usually implies high porosity and, consequently, low density values; density is one of the two variables that we use in our analysis, the other being the magnetic susceptibility. In the maps of Figures 4 and 5 two, perpendicular yellow lines
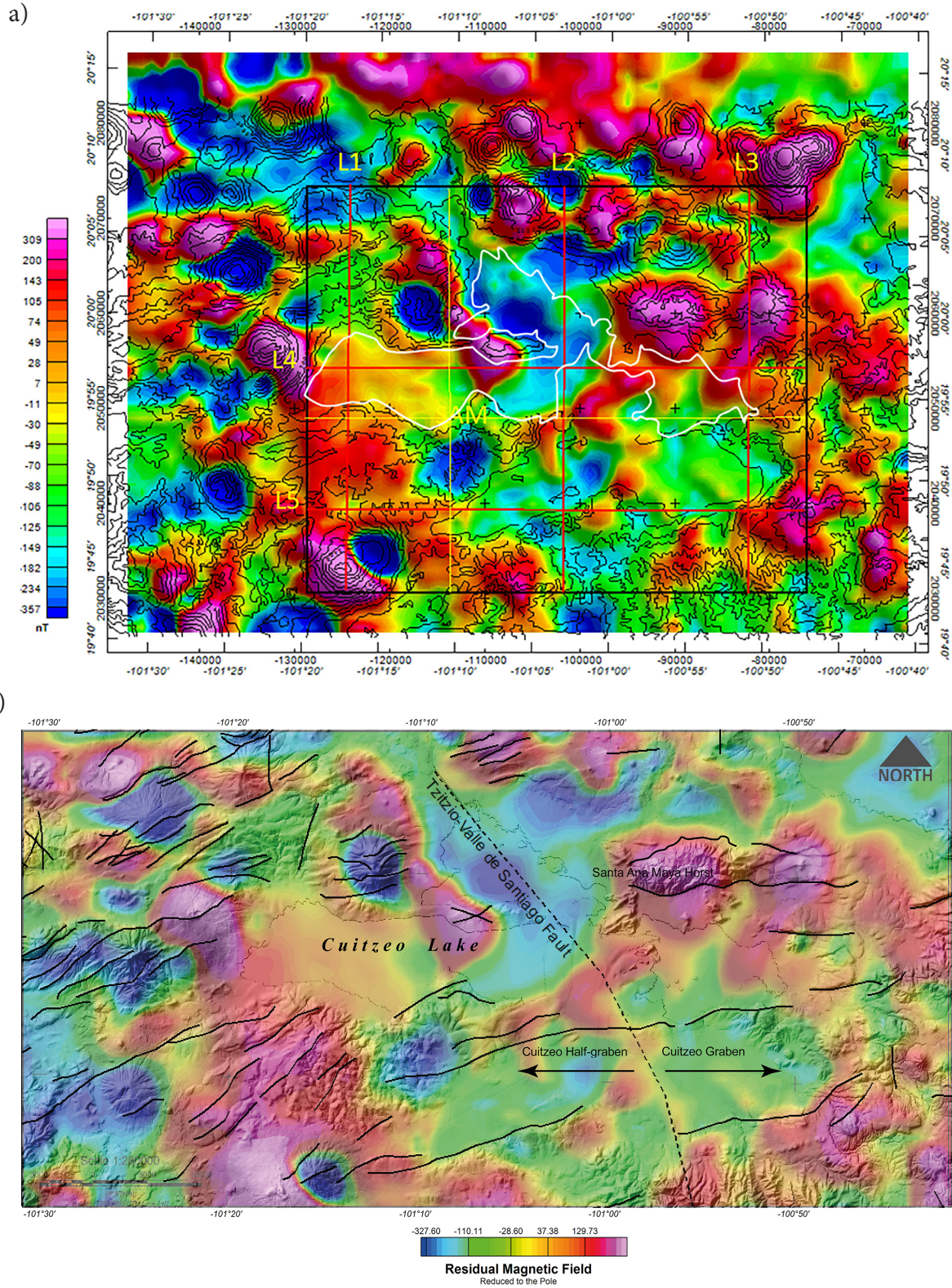
Figure 4. a) Magnetic map reduced to the pole of the Cuitzeo Lake region; elevation contours are shown for correlation, as well as the lake's outline (white). The black rectangle indicates the region in which a 3D inversion of the magnetic field is performed; the red lines (L1-L5) indicate where magnetic susceptibility cross-sections are obtained from such an inversion. SAM, Location of San Agustín del Maíz at the intersection of the two, perpendicular, yellow lines. b) Magnetic map reduced to the pole (Baranod and Naudy, 1964), superposed to the geologic map in Figure 3. Parameter values of the magnetic field: Inclination 47.60º, Declination 7.47º.
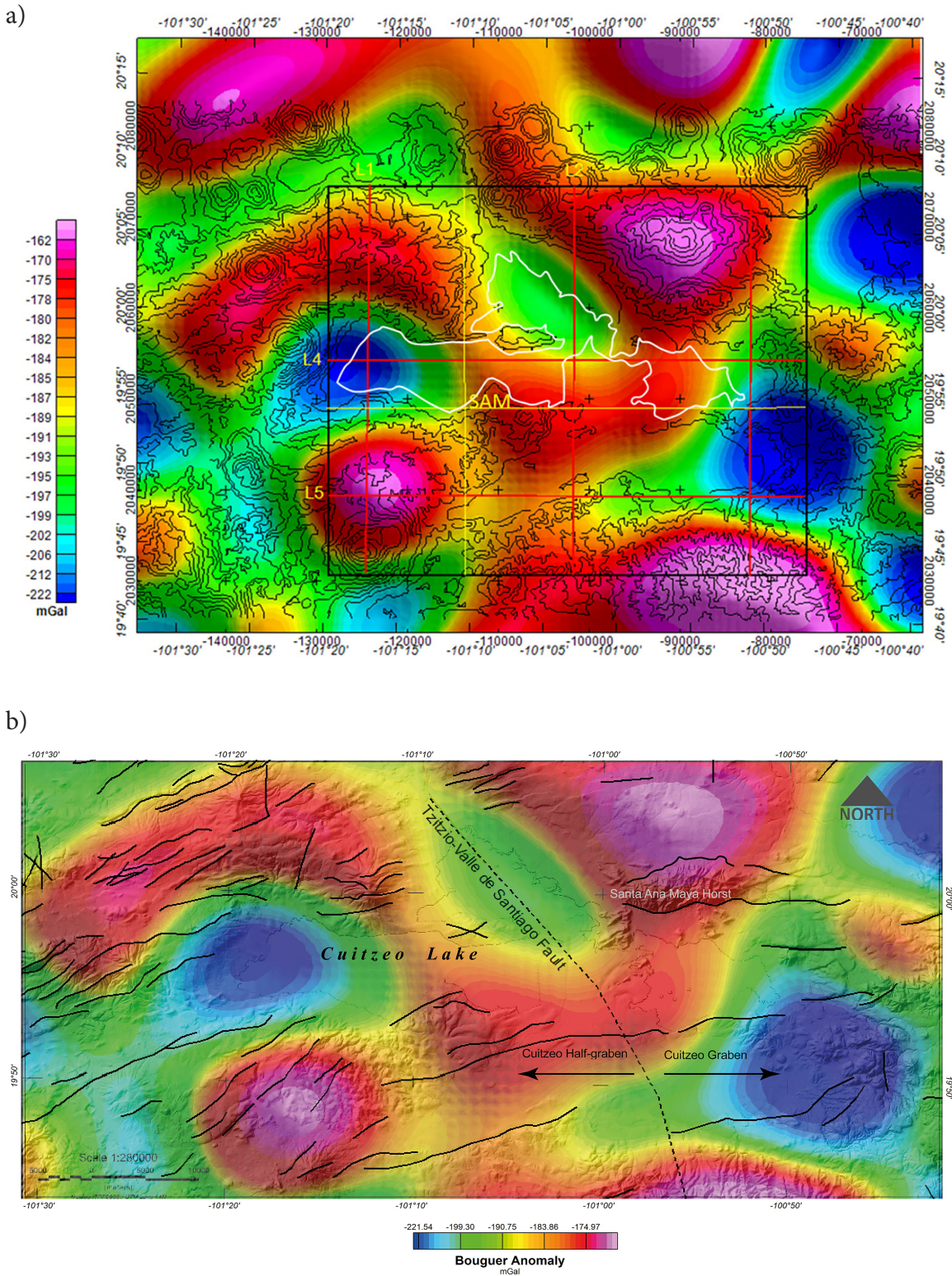
Figure 5. a) Bouguer anomaly (simple) map of the Cuitzeo Lake region; elevation contours are shown for correlation, as well as the lake's outline (white). The black rectangle indicates the region in which a 3D inversion of the gravity field is performed; the red and yellow lines indicate where density cross-sections are obtained from such an inversion; red and yellow lines are identified as in Figure 4. b) Bouguer anomaly map, superposed on the corresponding portion of the faults in the geologic map of Figure 3.
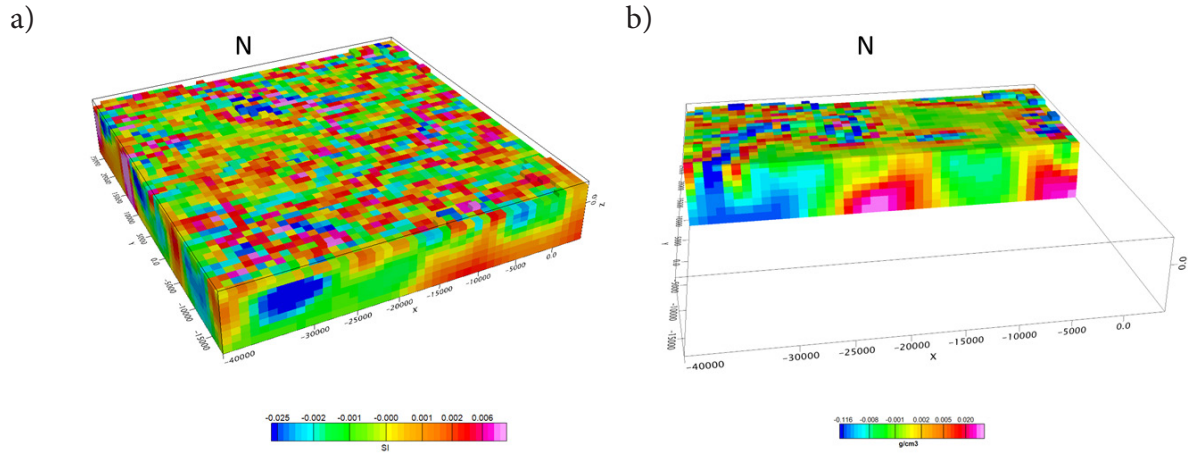
a)

b)

Figure 6. a) Full volume of the inverted model of the magnetic field reduced to the pole (Baranod & Naudy, 1964). b) E-W cross-section of the 3D gravity inversion showing the high-density (reds) and low-density (blues) voxels involved. Similar density cross-sections will be obtained along the yellow and red lines in Figure 5a, for the analysis of the density distribution. The mesh of points above the volume are the gravity stations used in the 3D inversion; the height of the stations is 500 m above the terrain. A similar set was used for inverting the magnetic data. Gravity scale + 2.67 g/cm³, magnetic scale +0.032 SI.
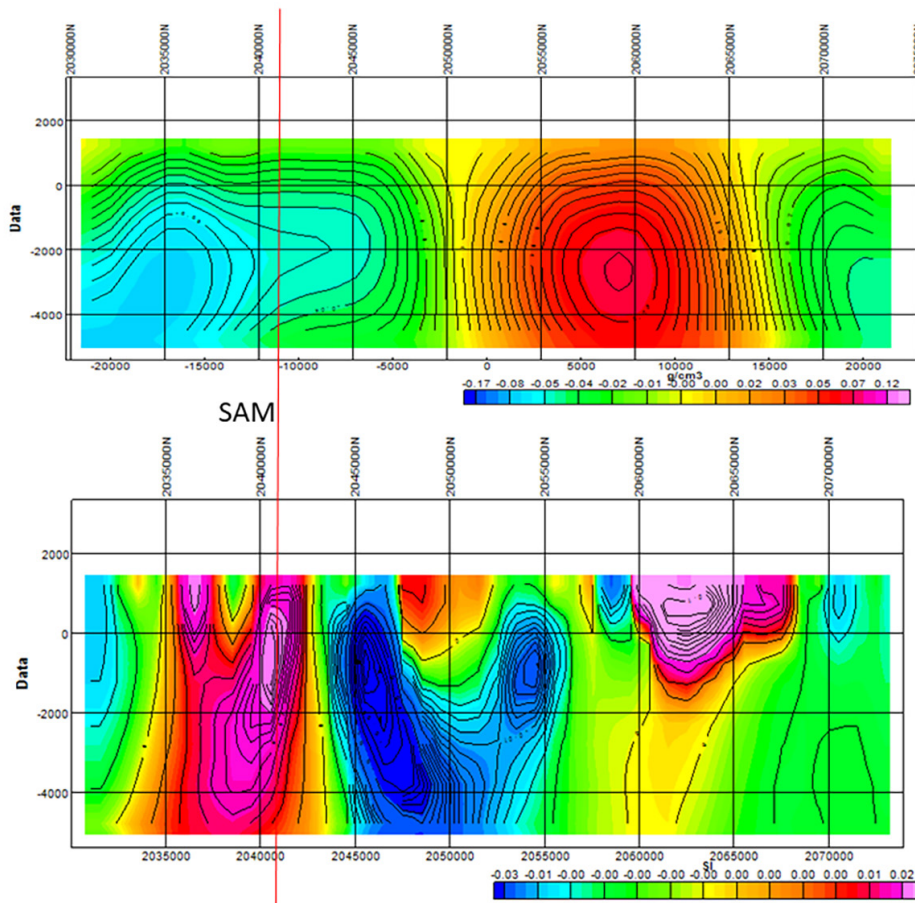

Figure 7. N-S cross-sections obtained from the 3D inversion of the gravity (above) and magnetic data crossing the location of San Agustín del Maíz (thin, red line). See Figures 4 and 5 for the location of the cross-sections. The horizontal scales are matched. Gravity scale + 2.67 g/cm³, magnetic scale +0.032 SI.

show the location of two cross- sections that intersect in the vicinity of SAM; the N-S and E-W cross-sections appear in Figures 7 and 8, respectively. In each instance the density section (in g/cm³) appears above, and the magnetic susceptibility (in SI units +0.032 SI.) appears below.

In Figure 7, the density cross-section shows an important low-density region centered at -3000 m extending to the N, with a minimum at -2000 m under the location of SAM, suggesting that the low-density region feeds the geothermal manifestations in SAM. The presence of thermal springs and siliceous sinter deposits west of SAM (Olvera-García *et al.*, 2020) tend to confirm our observations. We consider the association of low-density regions with high temperatures as favorable to geothermal sources, since it may contain fluids at high temperatures that decrease magnetic susceptibility, and low-density, porous materials allowing fluid circulation. Continuing northwards, there is a considerable block of high-density material. The magnetic susceptibility cross-section shows a chanel of low-susceptibility, rising from the bottom of the model (-5000 m) that emerges at

the location of SAM (thin, red line).

The boundary between the regions of high- and low-susceptibility regions is conspicuosly associated with the normal fault through SAM, reported by Olvera-García et al (2020); the region of minimum susceptibility extends down to -5000 m showing some obliquity and confirming that these are deep-seated faults. Given the associated thermal manifestations in the surface, we conclude that the low-susceptibility of this region arises from materials subject to high temperatures, probably reaching close to the temperature of the Curie isotherm (Ravat, 2000). The simultaneous presence of the low-density material, as shown by the density cross-section, and the outcropping region of low-susceptibility, suggest that the surface geothermal manifestations are fed from a deep source, extending below -5000 m. A bifurcation to the N, of the low-susceptibility conduit is observed starting at -3000 m, which also reaches close to the surface; this region also appears of geothermal potential and should be further analyzed by other means. A good portion of the high-density region is also occupied by high-susceptibility
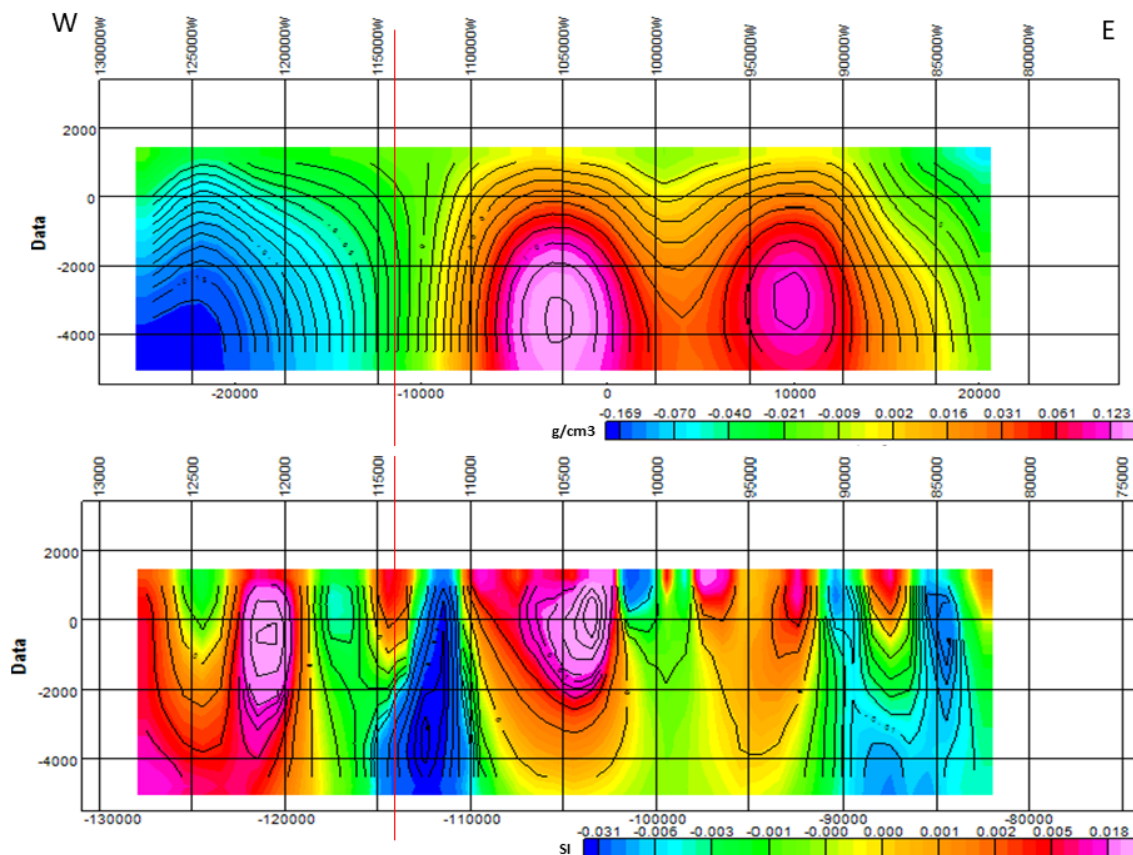

Figure 8. E-W cross-sections obtained from the 3D inversion of the gravity and magnetic data crossing the location of San Agustín del Maíz (thin, red line). See Figures 4 and 5 for the location of the cross-sections. The horizontal scales are matched. Gravity scale +2.67 g/cm³, magnetic scale +0.032 SI.

geologic formations; the joint effect of high density and high susceptibility suggests the presence of cold, volcanic materials emplaced significant time ago.

The density low observed in the southern portion of Figure 7, appears to extend westward in Figure 8, constituting a major anomaly in that region. The low-susceptibility region associated with the location of SAM (thin, red line) also appears bifurcated in this cross-section, hinting there is a circular distribution of low-susceptibility materials on the surface. The two density maxima correspond to two high-susceptibility regions. At the esatern end of the line, there is a similar distribution of low-density materials, with a shallow, central, high-susceptibility region, which is occupied by a density section, transitional between high- and medium-density.

We conclude that the density and magnetic susceptibility signatures around SAM are consistent with a region of high temperature of, at least 7 km depth and 20 km in length in the N-S direction, and 15 km in the E-W direction. With the help of X-ray analysis (DRX) Trujillo-Hernández, (2017) concludes that the abundant concentration of hydrothermally altered minerals, as well as the geologic evidence showing a high-degree of fracturing, mainly on the basaltic andesite lava flows, suggest that the chemical components travelled large distances, closing that the transport of hydrothermal fluids occurs mainly by infiltration.

With the experience gained analyzing the responses of the SAM region containing geothermal manifestations, we proceed to the analysis of L1-L5 cross-sections.
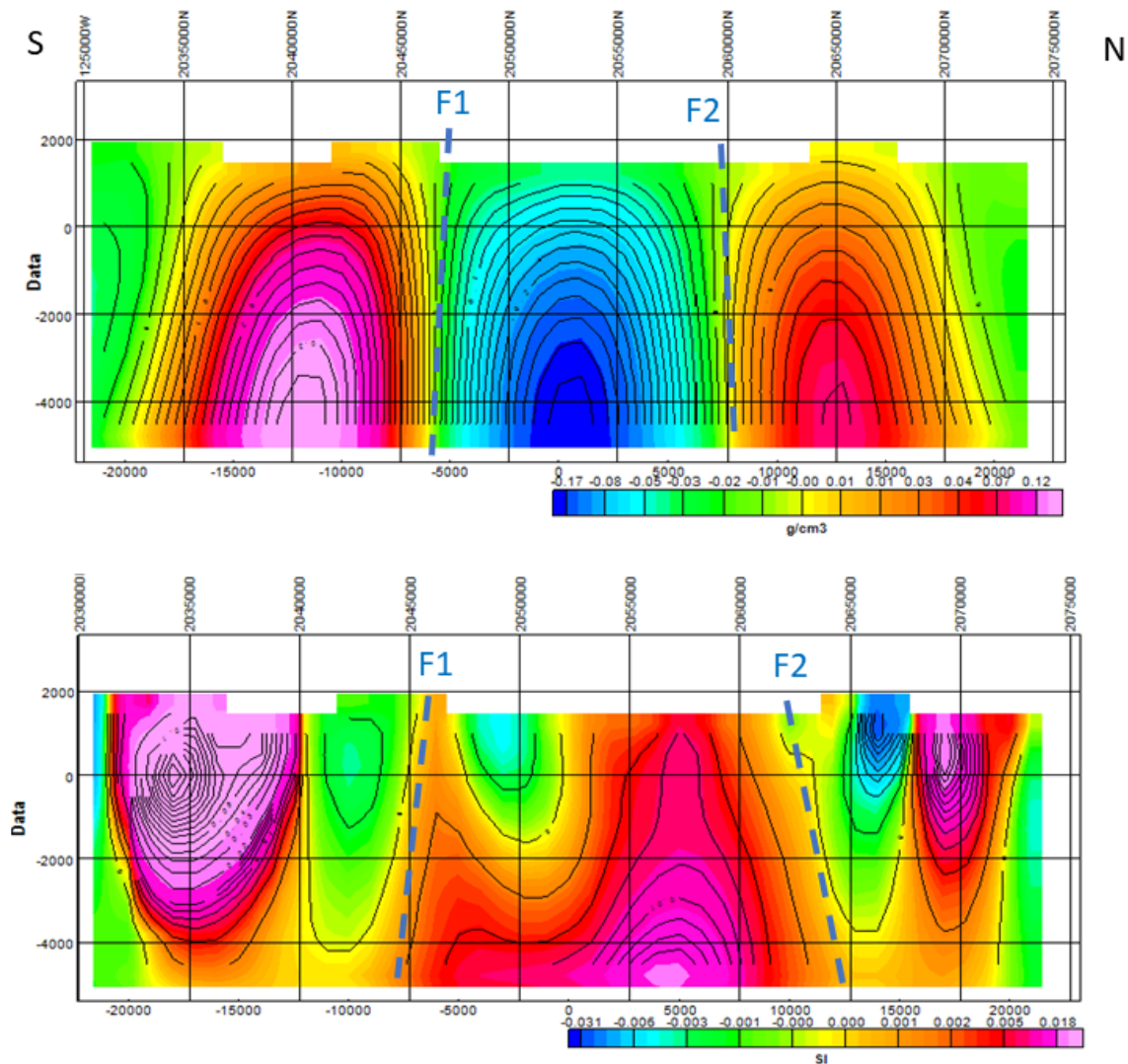

Figure 9. L-1, N-S cross-sections obtained from the 3D inversion of the gravity (above) and magnetic data. See Figures 4 and 5 for the location of the cross-sections. The horizontal scales are matched. F1 and F2 represent boundaries between contrasting properties in the cross-sections. Gravity scale $+2.67$ g/cm^3, magnetic scale $+0.032$ SI.

2) The N-S Lines

Here we analyze the group of three N-S lines labeled L1-L3 in Figure 4.

L1 is the westernmost line, oriented N-S. The density cross-section exhibits a large negative anomaly well constrained by two high-density regions with vertical boundaries F1, F2; it resembles a graben structure, but lacks an extended graben axis. The lowest density values are close to the 5 km depth, probably linked to the corresponding anomalies in the N-S and E-W cross-sections of SAM (Figures 7 and 8). The central portion of the magnetic susceptibility cross-section shows structural characteristics similar to those of the central anomaly of the density cross-section; that is, it has the same width and depth. The bounding limits F1 and F2 are followed by a low and a high susceptibility region, respectively. From these observations we conclude that the central region of this cross-section is a major anomaly of geothermal potential.

L-2 presents structural characteristics like those observed along L1. There is a main low-density region, not centered but slightly displaced to the N, also bounded by two high-density regions, whose boundaries also reach to the bottom of the cross-section. Given the density similarities between L1 and L2, and their proximity, one would tend to connect the main low-density anomalies; however, from Figure 5a one can see that they are separated by a region of high gravity values, which prevents such a connection. The corresponding region in the magnetic susceptibility cross-section, exhibits a bifurcation of the low-susceptibility region, similar to the one displayed in Figure 7, that surfaces at the F2 boundary, indicating that it also may represent the source of a potential geothermal area. Of particular interest is noting that this isolated anomaly is crossed
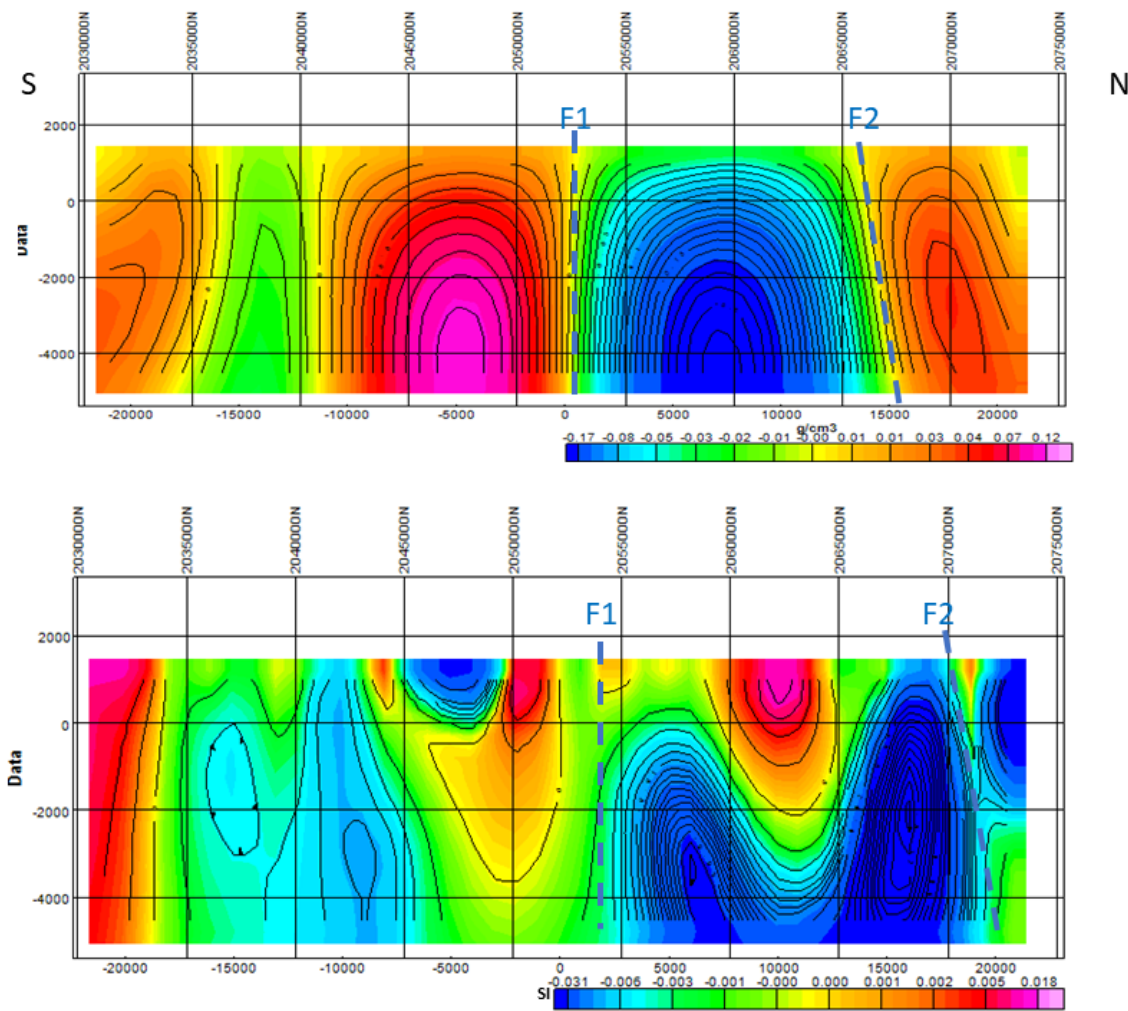

Figure 10. L-2, N-S cross-sections obtained from the 3D inversion of the gravity (above) and magnetic data. See Figures 4 and 5 for the location of the cross-sections. The horizontal scales are matched. F1 and F2 represent boundaries between contrasting properties in the cross-sections. Gravity scale $+2.67\,g/cm^3$, magnetic scale $+0.032\,SI$.

by the Tzitzio-Valle de Santiago fault (see Figure 3), which may have facilitated the intrusion of a heat source at depth.

According to Trujillo-Hernández (2017) this fault, that cuts through Cuitzeo Lake, is the most important NNW-SSE construct, defined as an old, buried fold-fault structure, responding to the present stress regime as a right-lateral fault. This system is presently active, cutting from old Early Miocene formations to Recent soils and volcanoclastic formations.

This line samples the Cuitzeo graben (Figure 5b) from S to N. It presents a different behavior from those observed at L1 and L2, since the low-susceptibility region at the center of the section corresponds with a high-density region in the density section, flanked by low-density areas which, in turn, correspond to two high-susceptibility regions.

3) The E-W cross-sections

Lines 4 and 5 in Figure 4 are the two E-W cross-sections that appear in Figures 12 and 13, respectively.

L4 crosses the study area from W to E (Figure 4). Regions of low and high density alternate in the cross section, corresponding to the low and high values of the BA; the density cross-section shows that transitions from low- to high-density regions reach vertically the full depth of the inversion (from +2000 m to -5000 m), suggesting a tectonic control of the distribution of geologic materials. The magnetic susceptibilty cross-section shows that the portion corresponding to the high-density section has low-susceptibility regions similar to those observed in SAM (Figure 7), also divided by a small, high-susceptibility region,
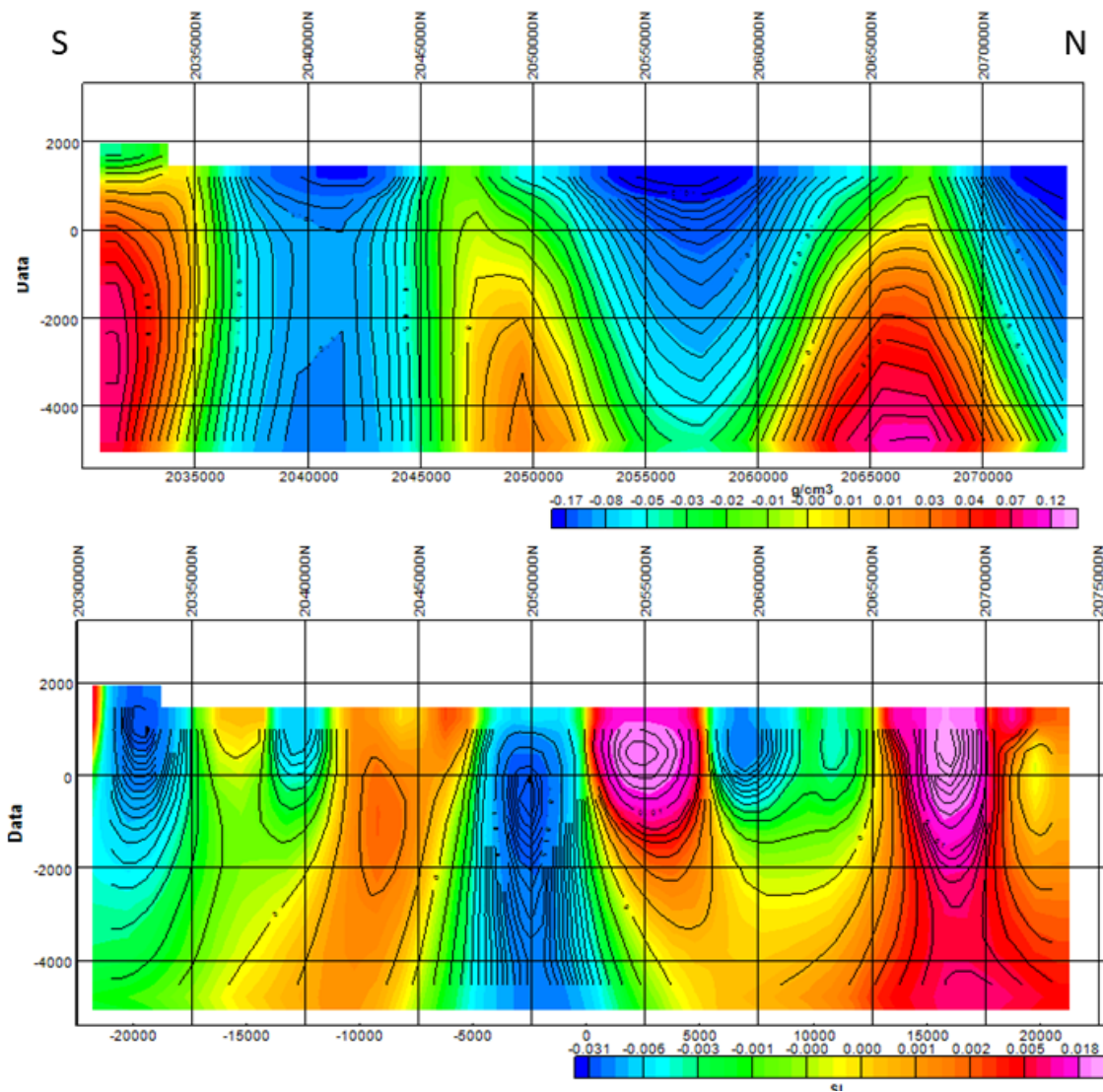

Figure 11. L3 N-S cross-sections obtained from the 3D inversion of the gravity (above) and magnetic data. See Figures 4 and 5 for the location of the cross-sections. The horizontal scales are matched. Gravity scale +2.67 g/cm³, magnetic scale +0.032 SI.

suggesting that this anomaly distribution occupies a considerabe area of this region. Close to the end of the line (88000E or 100º-53') in the N side, a negative low-susceptibility region with deep roots reaches the surface; it corresponds to a medium-density region, which could also be considered a potential exploration target for geothermal objectives, since it appears close to the south fault of the Santa Ana Maya horst (Figure 5).

L5 samples the S portion of the study area from W to E. The pattern observed in L4 regarding the vertical boundaries between high- and low-density regions is observed in two thirds of the length of L5, noticing a considerable departure from this behavior in the N portion of this section, where low density distributions predominate. There, the minimum of the low-density portion is located at -4000 m depth; this anomaly outcrops almost directly above this minimum. At the E end of L5 there is another

outcropping region of low density, except it has density values like those observed at the anomaly located at -4000 m, making it another potential target for geothermal evaluation.

The magnetic susceptibility cross-section shows a low-susceptibility region well constrained by high-susceptibility regions, extending from the surface to -5000 m depth, corresponding with the high-density region. At the E end of the line, there is a good match of shallow, low-susceptibility regions with the low-density regions reported above as potential geothermal targets, reinforcing such a statement.

4) Geosurfaces

A geosurface is obtained from an inverted volume, as the region in which the volume has a constant value, in g/cm³ if the
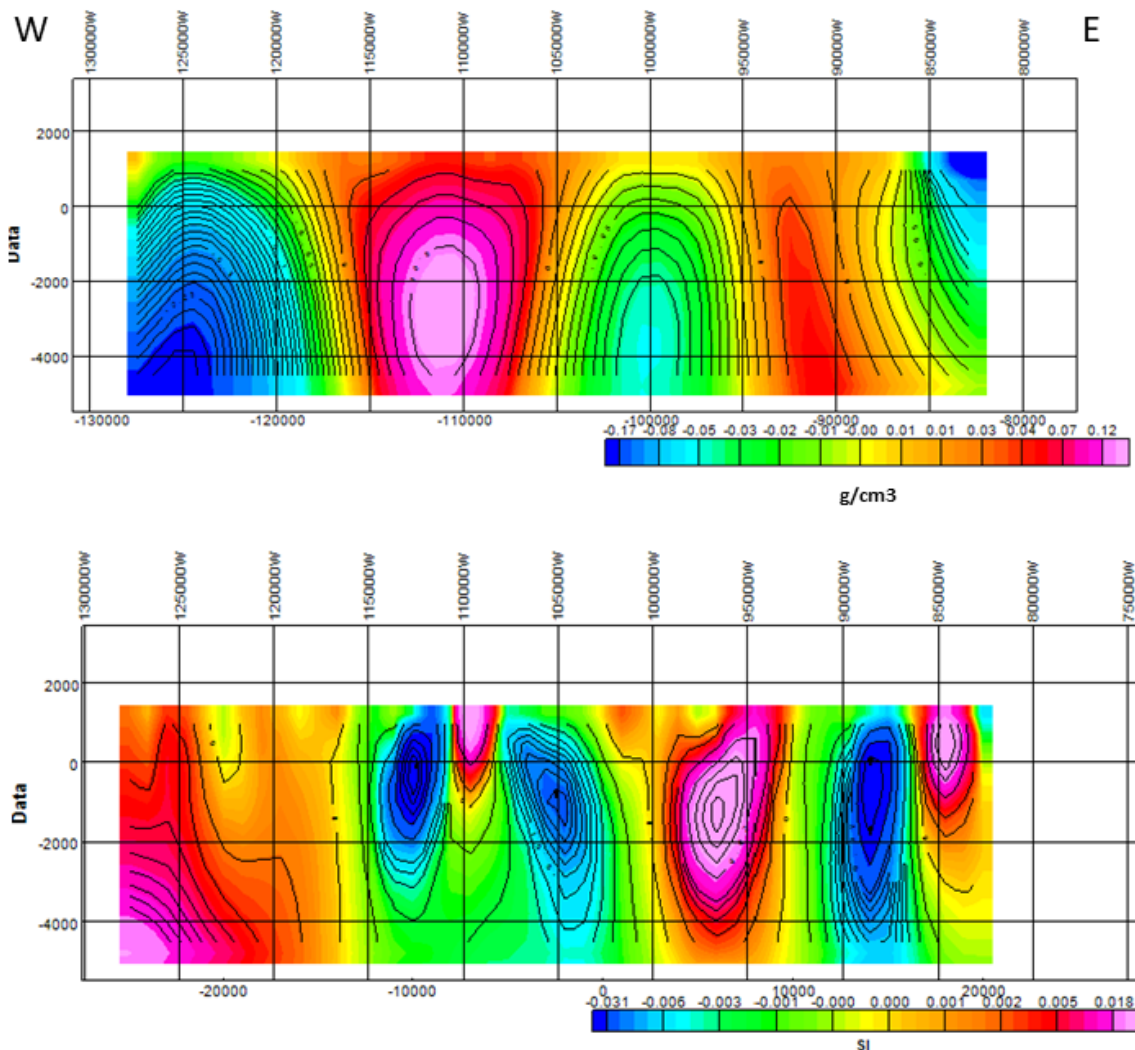

Figure 12. L4 in Figure 4, showing the cross-sections of density and magnetic susceptibility along the E-W direction; the horizontal scales are the same. Gravity scale + 2.67 g/cm³, magnetic scale +0.032 SI.

inverted volume is a density distribution, and in SI units if it is a distribution of magnetic susceptibilities. Geosurfaces complement observations made with the cross-sections.

A set of calculated density geosurfaces is in Figure 14; they range from 2.76 to 2.46 g/cm³; in the calculation, the whole inverted volume is scanned to determine where those density values are located and, then plotted. The blue surfaces are close to the vertical and, in the present case, extend from the surface to the bottom of the inverted volume, or about 7 km in depth. We searched for lower densities, down to 2.46 g/cm³, finding only two locations in which they are present; they are labeled as A1 and A2 in Figure 14. A1 is located close to the geothermal manifestations in SAM, and we submit that this is most likely the heat source feeding these geothermal manifestations. In A2 the green surface is cut to allow looking at the orange surface; below it, we could not locate a magenta surface. A2 is traversed

by the Tzitzio-Valle de Santiago fault (Figure 5) and we propose that it should be considered a geothermal exploration target, for its similarity with A1. The geothermal fluids can pass through the impervious cover owing to the persistent tectonic activity maintaining the permeability.

In Figure 14 there are four geosurfaces of different colors, corresponding to four density values. The geosurfaces in blue call the attention, since they start at the surface and end at the bottom (7 km) of the inverted volume, following vertical, or close to vertical inclinations; furthermore, they are thin, and cross the study area in various directions, restraining the regions of high gravity values, as seen in Figure 15, where we have superposed the geosurfaces to the BA map. We interpret them as vertical, boundary, or transitional regions, between high- and low-density regions, yielding the observed responses. Portions of these boundary surfaces are also present in the cross-sections presented
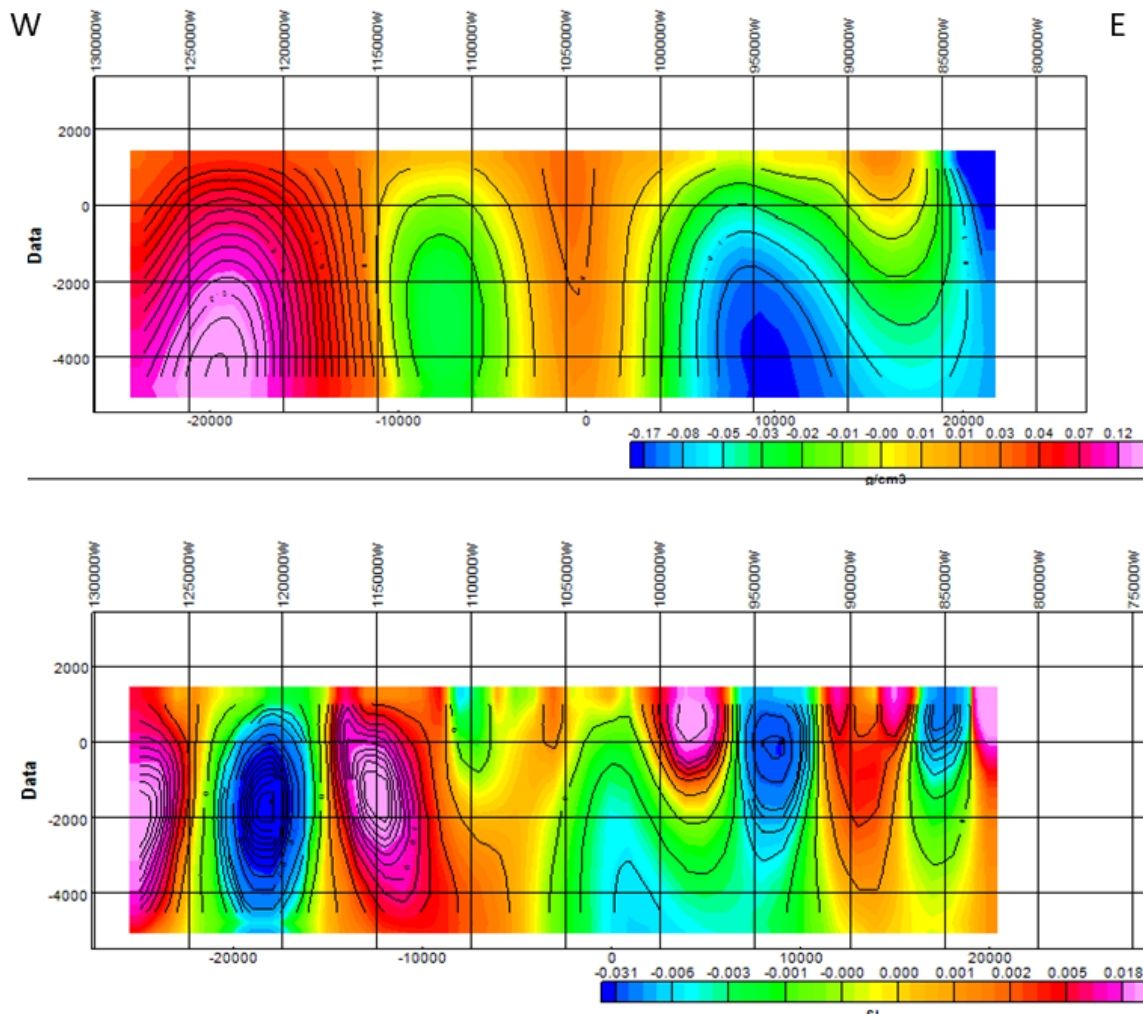

Figure 13. L5 in Figure 4 showing the cross-sections of density (above) and magnetic susceptibility, along the E-W direction; the horizontal scales are equal. Gravity scale +2.67 g/cm³, magnetic scale +0.032 SI.
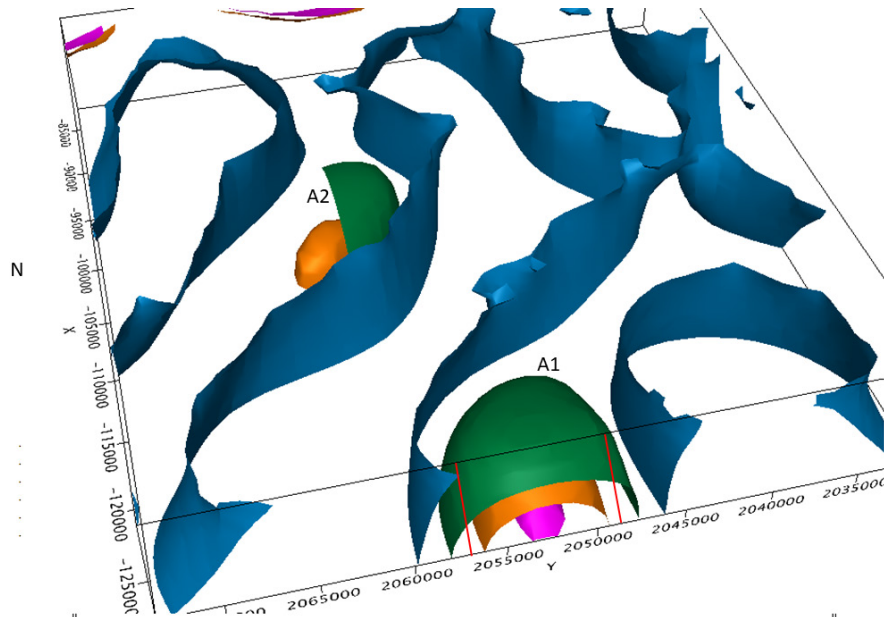
Figure 14. 3D display of geosurfaces for various densities (g/cm³): blue (2.76), green (2.66), orange (2.56), magenta (2.46). North is to the left; this view allows to appreciate how low-density varies with depth in anomaly A1; the green geosurface, in anomaly A2, is clipped to allow viewing the orange surface, no magenta surface is present. The brown, dashed line crossing the figure from N to S is the trace of the Titzio-Valle de Santiago fault. The red line is the outline of Cuitzeo Lake.

above; in some places they may be identified with faults bounding the low-density regions.

If we consider the superposition of the inverted results over the Bouguer anomaly map, in Figure 15, we note i) that the surface geothermal manifestations of SAM are located over one of these blue geosurfaces, and ii) that they are quite close to the anomalous density region A1, shown in section in Figure 14. Since there are only two anomalies with low-density characteristics in the inverted 3D region, A1 and A2, we infer that they are potential heat sources for geothermal fluids. The proximity of anomaly A1 to SAM, also illustrated in the density cross-section of Figure 6, tends to validate our inference. Although there appear to be no surface, geothermal manifestations in the region of anomaly A2, it should be considered a potential exploration target; the center of the anomaly is located 11 km E of Cuitzeo del Porvenir town, over the Tzitzio-Valle de Santiago fault (see Figure 3).

Figure 16 shows the vertical superposition of density geosurfaces, with some transparency, and susceptibility prisms of values between 0.042 and 0.012 SI. We observe two branches (NW and SE) and a central channel between them, oriented SW-NE; the latter shows a minor presence of prisms with such values. At present we cannot offer a hypothesis about the reason for this peculiar susceptibility distribution. The NW branch exhibits

concentrations of these prisms in the rim of A1 (at SAM) and in the location of A2 (see Figure 15), allowing the association of these susceptibility concentrations with such anomalous regions. The largest concentration of prisms in the SE branch may be associated with the eastern portion of L4 (Figure 12).

5) 2D model

To complement these results and discussion, we calculated several 2D models to ascertain the regional structural characteristics of the area; an example appears in Figure 17 displaying the resulting model along L1. It shows that andesitic formations dominate the region and comprise the high-density regions, whilst the central portion contains conglomerates and sediments of approximately 500 m depth, overlaying a volcanic formation. The deepest layer is the granitic basement. Andesites appear to be the geologic formations sealing the geothermal fluids heated by intrusions. Tectonic movements and geologic faults must create the paths through which these fluids reach the surface at several locations. In particular for this model, the SW-NE fault system identified in Figure 3 intersecting Cuitzeo Lake, with one of its components going through SAM region, appears to be the one controlling fluid migration.
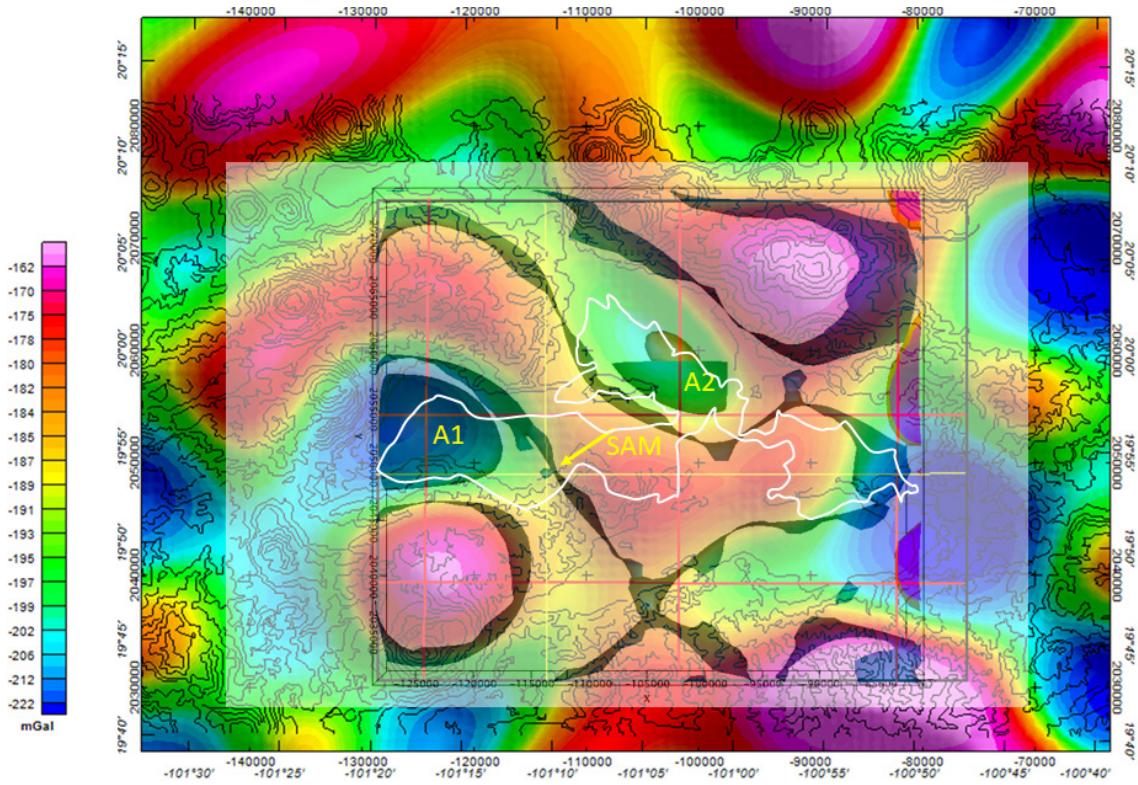
Figure 15. Vertical view of the geosurfaces obtained from the 3D gravity inversion, superposed (gray rectangle) on the BA map. A1 and A2 are the anomalies indicated in Figure 14. Red and yellow lines are labeled in Figure 4. The lake's outline in white.
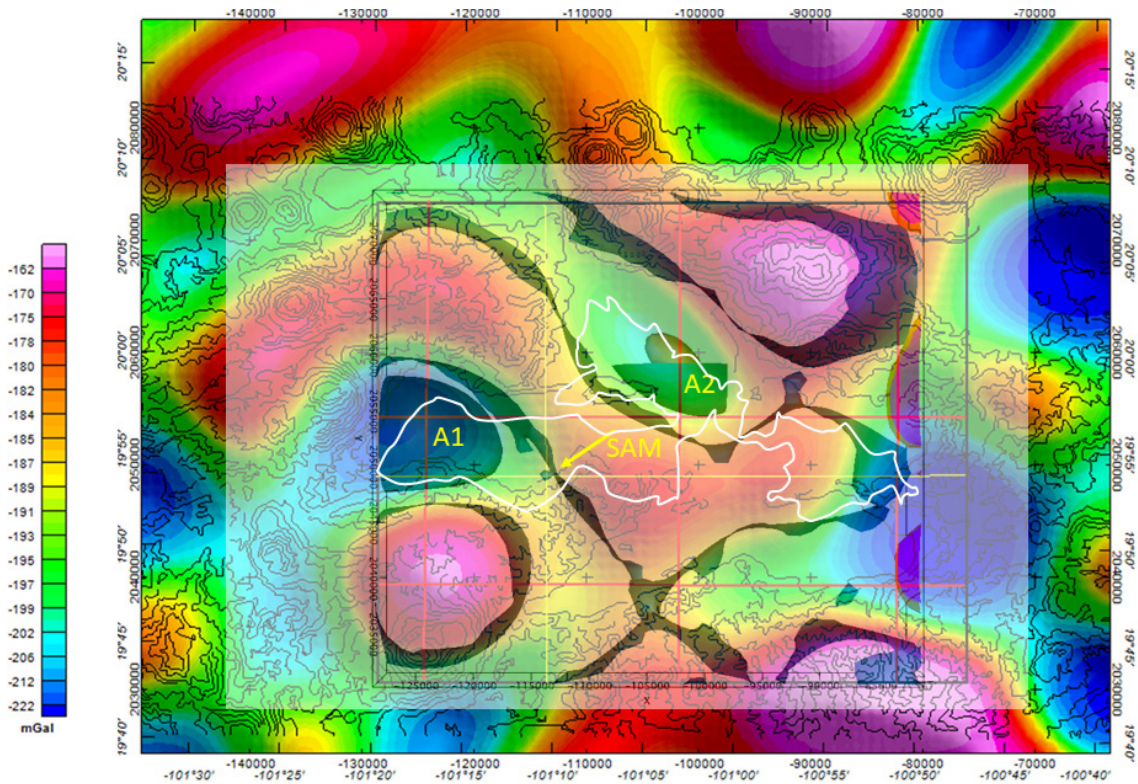

Figure 16. On the BA map we superposed the density geosurfaces and selected magnetic susceptibility prisms in the inverted region (gray rectangles). Magnetic susceptibility between 0.042 and 0.012 SI; the latter are the darker prisms.
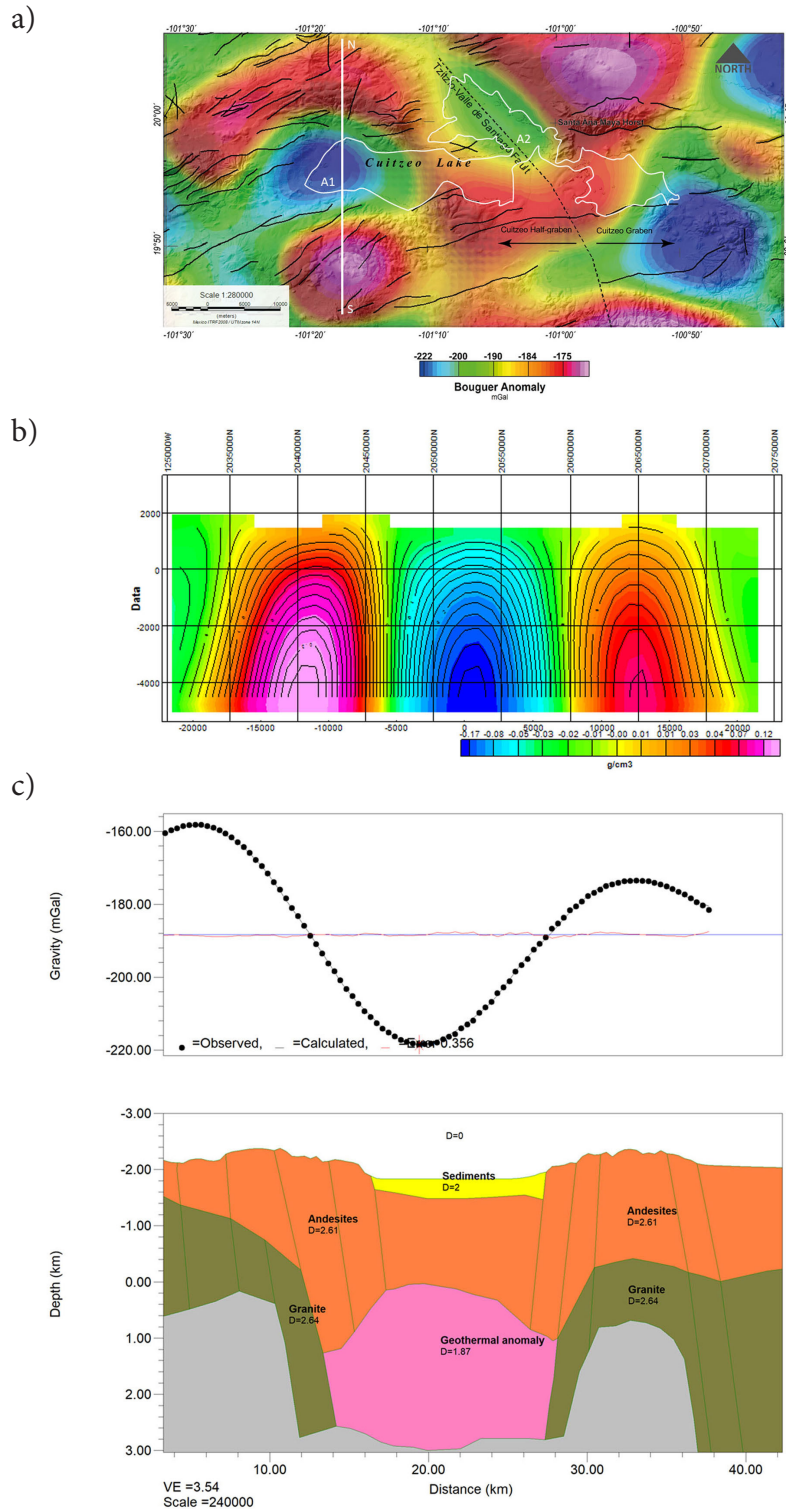
Figure 17. Two-dimensional gravity model along L1. a) N-S line L1 in which the model is calculated; volcanic products dominate the background. The Bouguer anomaly is superposed to a topography map (Figure 5) where several locations are identified, b) cross-section derived from the inverted density volume with a resolution of 1000 m, and c) 2D model 5 km in depth identifying geologic formations along the cross-section; distributions of Miocene to Quaternary andesitic lavas and dacitic ignimbrites described in Figure 3. A region, designated geothermal anomaly, is emplaced below sea level (0 m elevation) coinciding with A1 in Figure 14; an intrusive body may be responsible for the graben-like structure in the surface, and for the location of a low-density, high-temperature region. We define the geothermal anomaly as the joint occurrence of heated regions, fluid sources, and confining geologic structures.

Conceptual model

A conceptual model is shown in Figure 18, of an intrusive body causing the materials and fault distribution in the model of Figure 17, particularly the downward displacement of the region corresponding to Cuitzeo Lake. This intrusive is also the heat source for the geothermal manifestations. Motion along geologic faults would assist the flow of geothermal fluids reaching the surface.

Conclusions

The 3D inversion of gravity and magnetic data provided volume distributions of density and magnetic susceptibility that reproduced the observed fields within 5 percent of the respective standard deviations. From these results, we extracted cross-sections and geosurfaces that allowed the location of regions of potential geothermal interest. Analysis of two perpendicular cross-sections at a location with surficial geothermal manifestations (SAM) provided criteria that were used to analyze the whole inverted volume. We established that vertical boundaries between neighboring density and magnetic susceptibility regions, often extended throughout the entire thickness of the cross-sections (7 km), suggesting that such boundaries may be associated with deep geologic faults. We propose that the SW-NE trending fault system in Figure 3, is responsible for geothermal fluid migration in the SAM region. With these results, however, we cannot establish a uniform criterium, such as the association of low-density regions with regions of low susceptibility, to establish the existence of geothermal sources. We found zones in which, in addition to the above combination, regions of high density and low magnetic susceptibility, or high density and high susceptibility, may also represent potential geothermal targets in the surveyed region. More research is needed in this direction to characterize regions of geothermal potential. Concurrence of other geologic and geophysical methods will help refine the location of geothermal targets.

We conclude that the detection of geothermal exploration targets, using gravity and magnetic fields, is viable when adequate data sets are used; however, we recognize that, given the nature of the potential fields, results should be taken only as indications
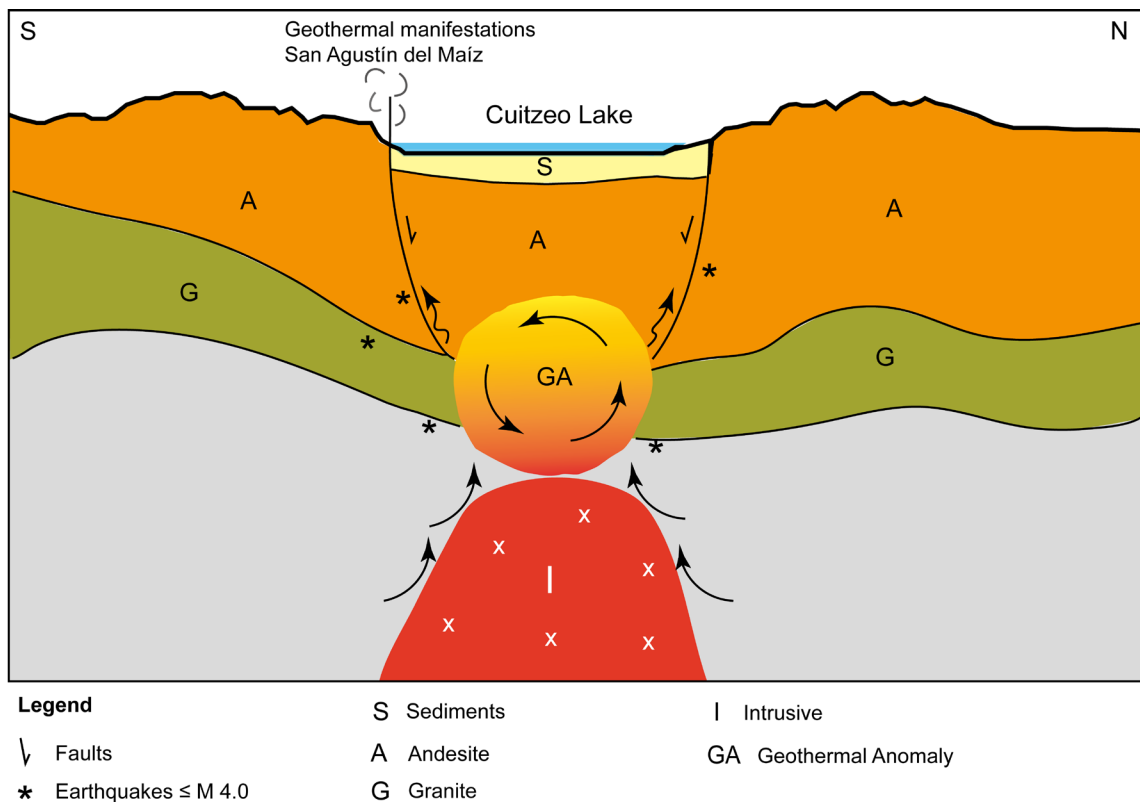

Figure 18. Conceptual model of the geothermal system feeding San Agustín del Maíz, in Cuitzeo Lake. The intrusive body heats the geothermal anomaly; its emplacement induces motion along the fault system, which in turn generates small magnitude earthquakes. Units described as sediments, andesite, and granite are only indicative of the type of rocks located in those regions. The gray region represents basement rocks containing an igneous intrusion I.

of the existence of such regions. Additional exploration methods should complement the results presented in this contribution. The advantage of using Potential Methods in exploration geophysics is that data is often available free, and large areas can be explored with limited resources before more costly methods can be applied. Data resolution should also be of primary concern when using this methodology; higher-resolution data sets will allow for a finer location of potential targets.

Declaration of Competing Interest

The authors declare that they have no known competing financial interests or personal relationships that could have influenced the work reported in this paper.

Authors statement

Both authors participated in conception and structure of the paper's lineaments. ER contributed mainly to the geological facets and RA in the geophysical analysis and interpretation of the data. Among them wrote and approved the final version.

Acknowledgments

References

Alvarez, R. & Camacho, M. (2023). Plumbing System of Hunga Tonga Hunga Ha'apai Volcano. *Journal of Earth Science,* 34(3): 706–716. **https://doi.org/10.1007/s12583-022-1792-0**

Alvarez, R. & Yutsis, V. (2015) Southward Migration of Magmatic Activity in the Colima Volcanic Complex, Mexico: An Ongoing Process. *International Journal of Geosciences, 6*, 1077-1099. **http://dx.doi.org/10.4236/ijg.2015.69085**

Alvarez, R & Yutsis, V. (2017) Potential fields modeling of the Serdán Oriental basin, Eastern Mexico. *Jour. South American Earth Sci.* **80** (2017) 375-388.
https://doi.org/10.1016/j.jsames.2017.10.003

Baranod, V. & Naudy, H. (1964). Numerical calculation of the formula of reduction to the magnetic pole. *Geophysics*, 29, 67-79.

Barthelmes, F. & Kohler, W. (2016). International Centre for Global Earth Models (ICGEM), in: Drewes, H., Kuglitsch, F., Adam, J. *et al.*, The Geodesists Handbook , 2016. *J. Geod.* 90 (10), 907–1205. **https://doi.org/10.1007/s00190-016-0948-z.**

Camacho, M. & Alvarez, R (2021) Geophysical modeling with satellite gravity data: EIGEN6C4 vs GGMplus. *Engineering*, **13**, 690-706. **https://doi.org/10.4236/eng.2021.1312050**

Correa-Gómez, J. G. (2019). Petrophysical characterization of a litofacies of the Cuitzeo, Michoacan ignimbrite sequence (in Spanish). Universidad Nacional Autónoma de México. Morelia City.

Ellis, R.G., de Wet, B. & Macleod, I.N. (2012) Inversion of Magnetic Data for Remnant and Induced Sources. Australian Society of Exploration Geophysicists, Extended Abstracts 2012, 1-4, Melbourne.

Ferrari, L. (2000). Advances in the knowledge of the Transmexican Volcanic Belt during the last decade (In Spanish). *Boletín de La Sociedad Geológica Mexicana, 53*(1), 84–92. **https://doi.org/10.18268/BSGM2000v53n1a5**

Ferrari, L., Orozco-Esquivel, T., Manea, V., & Manea, M. (2012). The dynamic history of the Trans-Mexican Volcanic Belt and the Mexico subduction zone. *Tectonophysics, 522–523*, 122–149. **https://doi.org/10.1016/j.tecto.2011.09.018**

Garduño-Monroy, V. H., Pérez-López, R., Israde-Alcantara, I., Rodríguez-Pascua, M. A., Szynkaruk, E., Hernández-Madrigal, V. M., García-Zepeda, M. L., Corona-Chávez, P., Ostroumov, M., Medina-Vega, V. H., García-Estrada, G., Carranza, O., Lopez-Granados, E., & Mora Chaparro, J. C. (2009). Paleoseismology of the southwestern Morelia-Acambay fault system, central Mexico. *Geofísica Internacional, 48*(3), 319–335. **https://doi.org/10.22201/igeof.00167169p.2009.48.3.29**

Gómez-Tuena, A., Orozco-Esquivel, M. T., & Ferrari, L. (2007). Igneous petrogenesis of the Trans-Mexican Volcanic Belt. *Special Paper of the Geological Society of America, 422*(303), 129–181. **https://doi.org/10.1130/2007.2422(05)**

Gómez-Vasconcelos, M. G., Garduño-Monroy, V. H., Macías, J. L., Layer, P. W., & Benowitz, J. A. (2015). The Sierra de Mil Cumbres, Michoacán, México: Transitional volcanism between the Sierra Madre Occidental and the Trans-Mexican Volcanic Belt. *Journal of Volcanology and Geothermal Research, 301*(June 2016), 128–147. **https://doi.org/10.1016/j.jvolgeores.2015.05.005**

Gómez-Vasconcelos, M. G., Macías, J.L., Avellán, D. R., Sosa-Ceballos, G., Garduño-Monroy, V. H., Cisneros-Máximo, G., Layer, P. W., Benowitz, J., López-Loera, H., López, F. M., & Perton, M. (2020). The control of preexisting faults on the distribution, morphology, and volume of monogenetic volcanism in the Michoacán-Guanajuato Volcanic Field. *Bulletin of the Geological Society of America, 132*(11–12), 2455–2474. **https://doi.org/10.1130/B35397.1**

Gómez-Vasconcelos, M. G., Avellán, D. R., Soria-Caballero, D., Macías, J. L., Velázquez-Bucio, M. M., Jiménez-Haro, A., Israde-Alcántara, I., Garduño-Monroy, V. H., Ávila-Olivera, J. A., Figueroa-Soto, Á. G., Cisneros-Máximo, G., & Cardona-Melchor, S. (2021a). Geomorphic characterization of faults as earthquake sources in the

Cuitzeo Lake basin, central México. *Journal of South American Earth Sciences, 109*(February), 103196. **https://doi.org/10.1016/j.jsames.2021.103196**

Gómez-Vasconcelos, M. G., Avellán, D. R., Soria-Caballero, D., Macías, J. L., Velázquez-Bucio, M. M., Jiménez-Haro, A., Israde-Alcántara, I., Garduño-Monroy, V. H., Ávila-Olivera, J. A., Figueroa-Soto, Á. G., Cisneros-Máximo, G., & Cardona-Melchor, S. (2021b). Geomorphic characterization of faults as earthquake sources in the Cuitzeo Lake basin, central México. *Journal of South American Earth Sciences, 109*(January), 103196. **https://doi.org/10.1016/j.jsames.2021.103196**

Guevara, R., Yutsis, V., Varley, N., Almaguer, J., Calderón-Moctezuma, A., & Guevara- Mansilla, O. (2021). *Geophysical determination of the Jalisco and Michoacán blocks boundary along the Colima graben. Journal of South American Earth Sciences*. **109**, 382 103208. **https://doi.org/10.1016/j.jsames.2021.103208**

Guevara-Alday, J. A. (2015). Geological and geophysical studies for the elaboration of a conceptual model of the geothermal reservoir of San Agustín del Maíz, Michoacán, México (in Spanish). Universidad Michoacana de San Nicolás de Hidalgo. Morelia, Mich. **http://bibliotecavirtual.dgb.umich.mx:8083/xmlui/handle/DGB_UMICH/5276**

INEGI (1993). Vectorial Data Model (in Spanish). Instituto Nacional de Estadística, Geografía e Informática. Ags., México. **https://sinegi.page.link/DLNP**

Ingram, D.M., Causon, D.M. & Mingham, C.G. (2003) Developments in Cartesian cut cell methods. *Math Comp Simulation*, 61 (3–6): 561–572.

Israde-Alcantara, I., & Garduño-Monroy, V. H. (1999). Lacustrine record in a volcanic intra-arc setting: the evolution of the Late Neogene Cuitzeo basin system (central-western Mexico, Michoacán). *Palaeogeography, Palaeoclimatology, Palaeoecology, 151*(1–3), 209–227. **https://doi.org/10.1016/S0031-0182(99)00024-3**

Macleod, I.N. & Ellis, R.G. (2013) Magnetic Vector Inversion, a Simple Approach to the Challenge of Varying Direction of Rock Magnetization. Australian Society of Exploration Geophysicists, Extended Abstracts 2013, 1-4, Melbourne.

NAMAG, (2002). North American Magnetic Anomaly Group. Magnetic Anomaly Map of North America. In: US Department of the Interior and US Geological Survey. Scale 1:10000000.

Olvera-García, E., Garduño-Monroy, V. H., Liotta, D., Brogi, A., Bermejo-Santoyo, G., & Guevara-Alday, J. A. (2020). Neogene-Quaternary normal and transfer faults controlling deep-seated geothermal systems: The case of San Agustín del Maíz (central Trans-Mexican Volcanic Belt, Mexico). *Geothermics, 86* (January), 101791. **https://doi.org/10.1016/j.geothermics.2019.101791**

Pola, A., Martínez-Martínez, J., Macías, J. L., Fusi, N., Crosta, G., Garduño-Monroy, V. H., & Núñez-Hurtado, J. A. (2016). Geomechanical characterization of the Miocene Cuitzeo ignimbrites, Michoacán, Central Mexico. *Engineering Geology, 214*, 79–93. **https://doi.org/10.1016/j.enggeo.2016.10.003**

Quintanar, L., Cárdenas-Ramírez, A., Bello-Segura, D.I., Espíndola, V.H., Pérez-Santana, J.A., Cárdenas-Monroy, C., Carmona-Gallegos, A.L. & Rodríguez-Rasilla, I. (2018). A seismic network for the Valley of Mexico: present status and perspectives. *Seismol. Res. Lett.* **89** (2A), 356–362.

Quintanar, L., Rodríguez-González, M., & Campos-Enríquez, O. (2004). A shallow crustal earthquake doublet from the Trans-Mexican Volcanic Belt (Central Mexico). *Bulletin of the Seismological Society of America* **94**, 845–855.

Ravat, D. (2000). Curie Temperature (Curie Isotherm). In Hancock, P.L.; Skinner, B.J. (eds.). Oxford Companion to the Earth. Oxford: Oxford University Press. pp. 202–203.

Suárez, G., Caballero-Jiménez, G.V. & Novelo-Casanova, D.A., (2019). Active crustal deformation in the Trans Mexican Volcanic Belt as evidenced by historical earthquakes during the last 450 years. *Tectonics* **38**, 1–19.

Trujillo-Hernández, N. (2017). Geological, geochemical and mineralogic study of the volcanic sequences of the southwest portion of Cuitzeo Lake, Michoacan, linked to the geotermal zone of San Agustin del Maiz (in Spanish). Universidad Michoacana de San Nicolás de Hidalgo. **https://doi.org/http://bibliotecavirtual.dgb.umich.mx:8083/xmlui/handle/DGB_UMICH/4391**